

An Iterative Approach of Hot Isostatic Pressing Tooling Design for Net-Shape IN718 Superalloy Parts

Khamis Essa¹, Raja Khan², Hany Hassanin³, Miren Aristizabal², Moataz M. Attallah², Roger C. Reed⁴

¹*School of Mechanical Engineering, The University of Birmingham, Birmingham*

²*School of Metallurgy and Materials, The University of Birmingham, Birmingham*

³*School of Mechanical and Automotive Engineering, Kingston University, London*

⁴*Department of Engineering Science, University of Oxford, Oxfordshire*

The final publication is available at Springer via <http://dx.doi.org/10.1007/s00170-015-7603-3>.

Abstract

Powder Hot Isostatic Pressing is a resource-efficient approach for netshape manufacture of high-value Nickel-based superalloy structures. One of the key challenges to its application is the availability of modelling tools that can predict the geometrical changes that occur during the consolidation process in order to design the tooling required. In this work, the utility of a finite element code, based on the plastic collapse model, was assessed. The finite element model was then combined with an optimisation toolbox to design (in an iterative process) the tooling required to accommodate the powder consolidation process. The model was validated for IN718 superalloy, using a demonstrator with complex features. Microstructural characterisation was also performed to assess the degree of densification. Although the finite element model did not account for creep deformation, good predictions were obtained. Nevertheless predictions of the dimensions of consolidated samples were obtained, which were typically within 1% of the observations, suggesting that plastic collapse accounts for 99% of the geometrical changes due to the densification process for the range of hot isostatic pressing parameters investigated.

Keywords: Hot Isostatic Pressing, Nickel-Based Superalloys, IN718, Finite Element Modelling, Tooling Design

1. Introduction

Machining from solid forgings is currently the traditional method for the production of many high temperature gas turbine components. Due to the increasing need for the gas turbines to run at higher temperatures, the introduction of high temperature materials such as Ni-based superalloys adds more difficulties in terms of machining and welding these materials, which considerably increases the cost of fabricating complex components by machining. Netshape powder Hot Isostatic Pressing (HIPping) is an alternative resource-efficient manufacturing approach that offers significant weight savings and lower buy-to-fly ratio [1], with minimal machining of the HIPped component.

In netshape HIPping, powder is filled into a canister (tooling), from a readily sacrificial material such as mild steel, which is designed to accommodate the large shrinkage that occurs for the powder during HIPping (typically 35% volumetric shrinkage). Before HIPping the container is out-gassed and sealed and then subjected to simultaneous isostatic pressure at an elevated temperature for several hours, after which the container is removed by machining or acid-etching. The porosity in the material is eliminated and the powder is compacted into a

fully dense, netshaped component. However, the ability to predict the shape change that occurs during HIPping, especially for complex-shaped components, is at present limited and the aim of the present work is to improve the ability to model this shrinkage in order to design the required tooling.

Finite Element (FE) modelling of HIPping is detailed in many reports. Shima and Oyane [2] proposed a plasticity theory for porous metals, which represents the basis for most of the powder consolidation modelling work. Cassenti [3] investigated HIPping modelling using an elasto-plastic large-deformation model with implicit thermal calculations. The ability of his model to predict the shape and geometrical changes was inadequate. Later, Nohara *et al.* [4] and Abouaf *et al.* [5-9] developed and adapted constitutive equations to account for elasticity, visco-plasticity, and thermal effects, and to model the mechanical behaviour of the powder. Similar FE models were also developed by Svoboda *et al.* [10-12], and Wikman *et al.* [13] who developed a combined material model that accounts for both granular and viscoplastic behaviours whereby the granular plasticity model accounts for the early extraordinary stage of the consolidation and the viscoplastic model accounts for the intermediate and later stages of consolidation. These models have been used for the prediction of the densification behaviour rather than tooling design, with a simulation time of about 4 days, making it unsuitable for tooling design optimisation. Using a similar approach, Gillia *et al.* [14] proposed a viscoplastic model that takes into account the strain hardening effect of the powder material. Recently, Yuan *et al.* [15] developed a FE model to predict the final dimensions of shaped part produced by HIPping Ti-6Al-4V powder, using the constitutive equations for plastic yielding, without considering the constitutive models that describe other densification mechanisms. This was justified based on the fact that more than 90% of powder density is gained within this instantaneous plastic yield mechanism which has relative concise formulation with fewer parameters involved as reported by Seliverstov *et al.* [16]. The developed model showed a very good agreement of more than 98% between the produced geometries and the predicted ones. Although the models developed by Yuan *et al.* [15] and Seliverstov *et al.* [16] were able to predict the final geometry of HIPed components, they were limited to a single guess of tooling design. Nevertheless, an iterative procedure for net-shape HIPping tooling design from initial guess with reasonable computational time is required.

In this paper, an FE model based on plastic collapse is used to predict the shape changes that occur during HIPping of an IN718 small demonstrator and integrated with an optimisation toolbox in order to design the required steel tooling that will achieve netshape HIPping. The demonstrator geometry was chosen to have a wide range of applications in the aerospace and nuclear sectors. The model was validated using geometrical scanning measurements and compared with that predicted by the model. To confirm the densification predictions of the model, microstructural investigations were also performed.

2. FE modelling of IN718 HIPping

2.1 Constitutive equations

Although powder densification during HIPping involves several mechanisms, a material model based on the pure plasticity theory would be justified to predict the final shape of the consolidated powder. This is based on the fact that more than 90% of powder densification during HIPping occurs via the instantaneous plastic yield mechanism which has a relatively concise formulation with fewer parameters involved, as reported by Yuan *et al.* [15] and

Seliverstov *et al.* [16]. In this investigation, a material model based on the modified Gurson's porous metal plasticity theory has been used. This material model defines the inelastic flow of the porous metal on the basis of a potential function ($\phi(\sigma, \rho)$) that characterises the porosity in terms of the relative density as shown in Equation (1).

$$\phi(\sigma, \rho) = \left(\frac{q}{\sigma_y} \right)^2 + 2q_1(1 - \rho) \text{Cosh} \left(-q_2 \frac{3P}{2\sigma_y} \right) - 1(q_3(1 - \rho))^2 = 0 \quad (1)$$

$$q = \sqrt{\frac{3}{2} S : S} \quad (2)$$

$$P = -\frac{1}{3} \sigma : I \quad (3)$$

where q is the effective Mises stress, S is the deviatoric part of the Cauchy stress tensor σ , P is the hydrostatic pressure, ρ is the relative density and q_1 , q_2 and q_3 are material parameters and were introduced by Tvergaard [17]. When $q_1 = q_2 = q_3 = 1$, Equation (1) reduces to the yield function originally proposed by Gurson's [18]. When $q_1 = q_2 = q_3 = 0$, Equation (1) reduces to the usual Mises stress.

The relation for the dependence of the elastic modulus on the relative density is shown in Equation (4) was proposed by Gillia *et al.* [14], who modified the model for cold compacted samples. Equation (5) establishes the dependence of the thermal conductivity upon relative density as proposed by Argento and Bouvard [19], which is applicable either at low or high density stages of the consolidation.

$$E(\rho, T) = E(1, T)(0.1 + 0.9\rho^{12}) \quad (4)$$

$$K_{eff} = K_s \left(\frac{\rho - \rho_o}{1 - \rho_o} \right)^{\frac{3}{2}(1 - \rho_o)} \quad (5)$$

where $E(\rho, T)$ is the modulus of elasticity of the solid at temperature (T), K_{eff} is the effective thermal conductivity, K_s is the thermal conductivity of the solid, and ρ_o is the initial relative density. The powder is modelled using the modified Gurson's porous metal plasticity theory while the mild steel container is modelled using the conventional Mises deformation equations. The material model described above were implemented in the implicit coupled temperature-displacement solver of the ABAQUS software. The thermo-elastic models, equation 4-5, were implemented into a user-defined model.

2.2 Numerical validation

A small demonstrator with complex features is shown in Figure 1(a). The proposed demonstrator consists of asymmetric cylindrical body that has straight and conical walls with a cylindrical solid boss, one body ring, and two edge flanges, the dimensions of which are shown in Figure 1(b).

Due to the iterative nature of the tooling design process, an initial guess of the tooling was proposed based on the powder characteristics (tap density), Figure 2. The tooling geometry was simplified to two axisymmetric and two corresponding finite element models were used as shown in Figure 3.

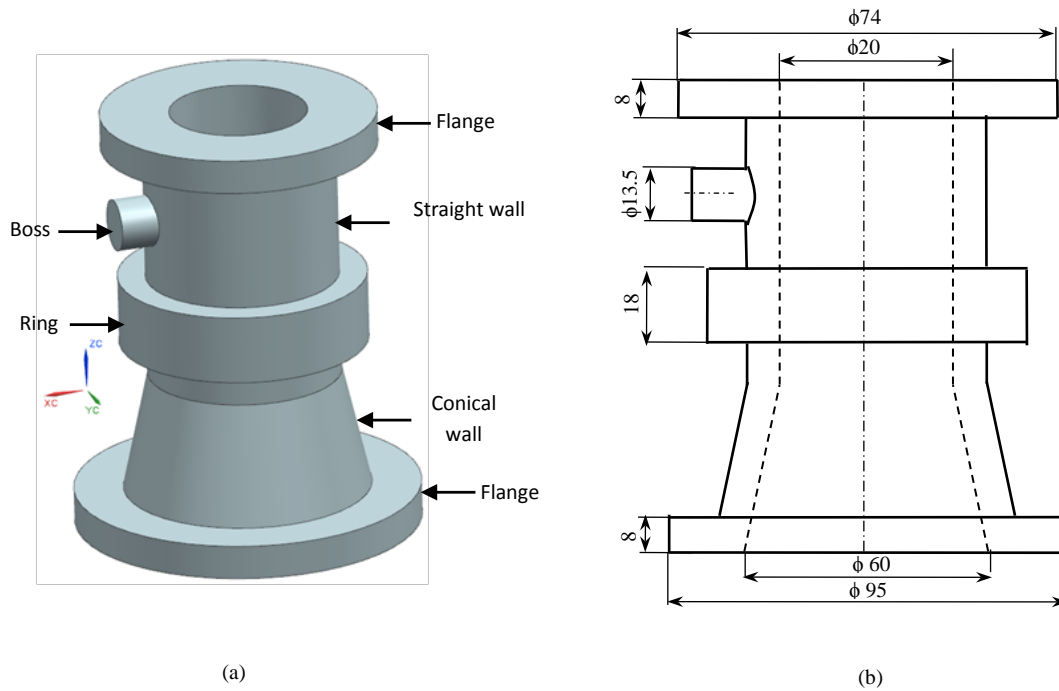


Figure 1. CAD drawing of the small scale demonstrator, (a) 3-D isometric view, (b) 2-D view with the dimensions (Dimensions are in mm)

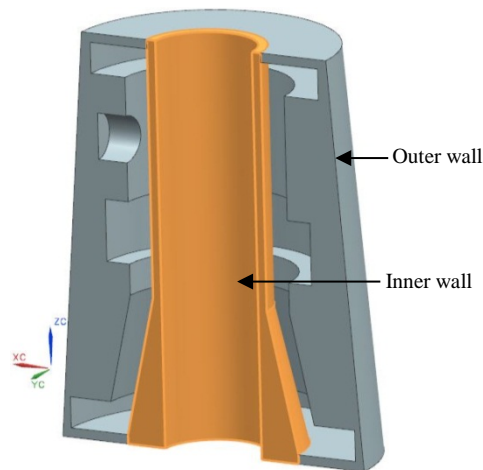


Figure 2. A sectional view showing one-half the tooling

In the FE model, the powder geometry was partitioned within the container geometry to provide a rigid contact between the powder and the surfaces of the container. The volume occupied by the powder, as well as the canister/tooling, were meshed using 8-node quadrilateral elements. The boundary conditions were set as follows: the pressure was applied to all free edges of elements and the temperature was prescribed for the nodes along these edges. A heating rate of $5^{\circ}\text{C}/\text{min}$ up to a subsolvus temperature (to avoid local melting of

certain phases) was used, with a dwell time of 4 hours. A cooling rate of 5°C/min was used. A pressure profile, similar in time to the temperature profile, was used, ramping the pressure up to 140 MPa. An axisymmetric displacement boundary condition was applied in the x-direction along the centre line.

Two different types of material descriptions were assumed in the computational model. Material model for the steel tooling is assumed to be thermal-elastoplastic, with temperature-dependent mechanical and thermo-physical properties, using AISI 1018 mild steel data [21]. The powder material was modelled using data for IN718. The thermo-physical properties and the flow curves for the compacted powder at different temperature and different strain rates are obtained from [20]. Preliminary modelling trials were performed on a simple geometry of solid cylinder using the described FE models to optimise and determine the material parameters q_1 , q_2 and q_3 and use their values for the modelling of the small demonstrator geometry.

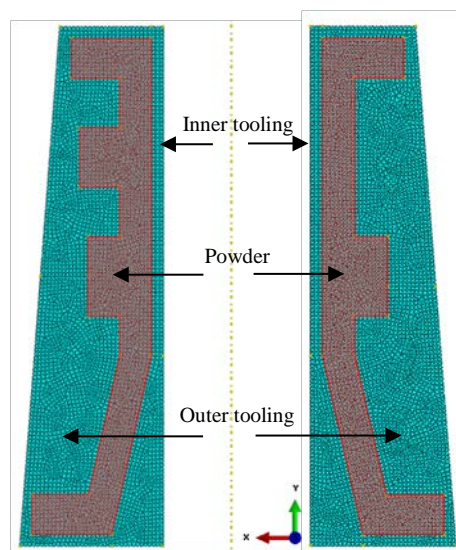


Figure 3. Axisymmetric FE mesh for the two sections representing the small scale demonstrator (green elements represent steel tooling and red elements represent powders)

Isight, a software product of SIMULIA provides a suite of visual and flexible tools for creating simulation process flow. Isight allows executing a variety of applications including ABAQUS software. It also enables the automation and control of process flows, design of experiments, and optimisation. To model the small demonstrator modelling, Isight was used to execute ABAQUS CAE and ABAQUS output database. The calculations were done in an iterative manner starting with the axisymmetric FE models from a guessed geometry. The target dimensions of the small demonstrator are first specified in an objective function of an optimisation module within Isight. After the first iteration, Isight executes the ABAQUS CAE to change the configurations of the inner and outer tooling and the output ABAQUS database (results file) to read the nodal coordinates of the consolidated powder. Some calculations are done on the executed nodal coordinates in order to determine the final dimensions of the small demonstrator after being HIPped. These dimensions are then compared with those specified in the objective function. If the required dimensions are not achieved, a new iteration will be performed until satisfying the objective function. Figure 4 shows the built-in process flow within Isight. The stable number of elements at which the solution was converged is 8940.

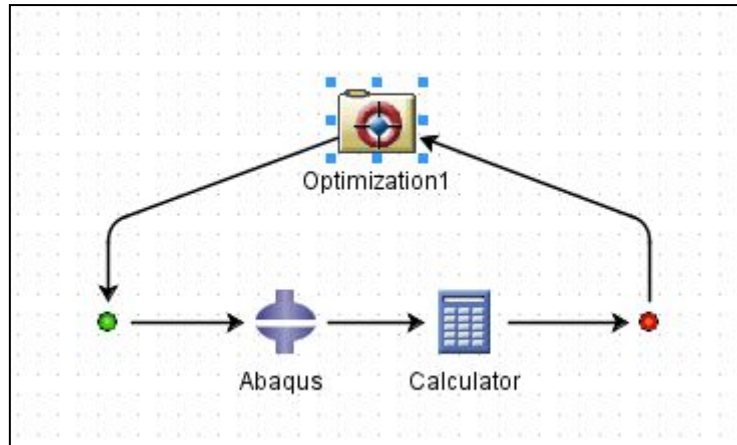


Figure 4. Isight process flow

3. Experimental

The design of the internal and external parts of the tooling was carried out in 3D CAD and their dimensions are determined by the optimised FE calculations.

A cylinder of AISI 1080 mild steel was machined to the tooling according to the CAD design. The tooling was subsequently filled with powder under mechanical vibration to achieve a uniform packing density, ensuring a consistent shrinkage during HIPping, and followed by outgassing for 24 hours, and sealing by arc welding.

The composition of the IN718 powder used in this study is shown in Table 1, with a size range of 45-150 μm . HIPping was performed in an EPSI HIP, with a maximum operating temperature up to 1450 $^{\circ}\text{C}$ and pressure up to 200 MPa. This unit consists of a furnace with molybdenum heating elements, a heat shield, a water-cooled pressure vessel and a gas compressor system. A computer system is used to control and monitor the temperature and pressure continuously inside the HIP furnace. Temperature control is within $\pm 3^{\circ}$ throughout the working zone.

Table 1. Chemical composition of IN718 (wt. %)

Alloy	Cr	Fe	Nb	Mo	Al	Ti	C	Si	Mn	Cu	Ni
IN718	18.7	19.09	5.04	3.01	0.43	0.94	0.011	0.04	0.01	0.01	Balance

For the used HIP cycle, temperature and pressure were ramped up together at rates of 5 $^{\circ}\text{C}/\text{min}$ and 0.6 MPa/min respectively, up to the desired HIPping temperature and pressure. The temperature and pressure are then held for 4 hours and finally they are ramped down at a controlled rate. To justify the material model used in this paper, a cylindrical canister filled with the same powder was HIPped at the same conditions, yet with zero holding time, to characterise the contribution of time-dependent densification. Finally, the tooling was then removed by pickling in Nitric acid solution. Figure 5 shows (a) the designed tooling obtained through the iterative FE model, (b) the tooling after HIPping, and (c) the as-HIPped demonstrator after acid pickling.

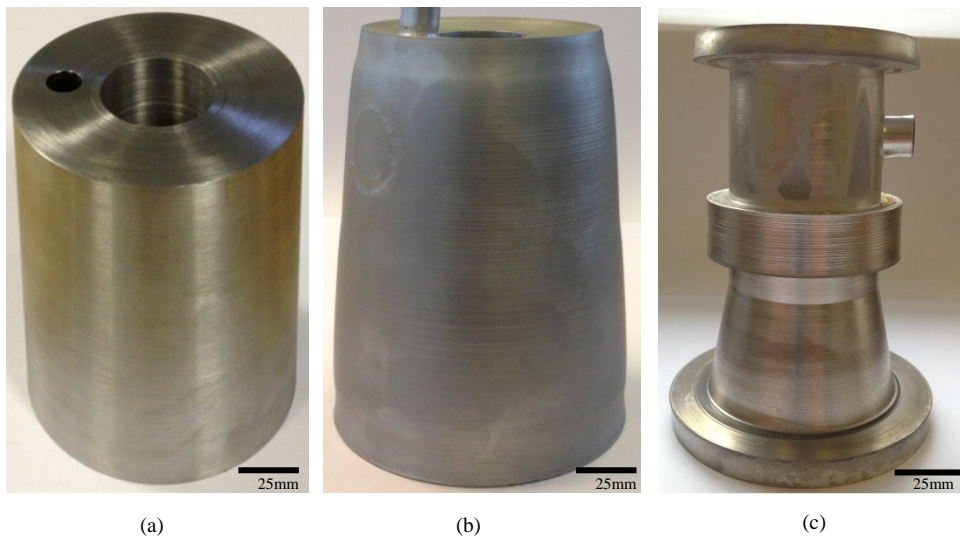


Figure 5. (a) The designed tooling, (b) as HIPped tooling and (c) as HIPped demonstrator after etching

Laser scanning was used to measure the shape of the as-HIPped demonstrator. Porosity evaluation was performed using a Leica DMRX optical microscope on as-polished samples while the microstructural characterisation was performed using Scanning Electron Microscopy (SEM). As the packing density of the powder is essential to feed the FE model, it has been calculated using mass to volume ratio after samples are being vibrated and the value has been fed to the FEA model. The measured packing (tap) density of this powder was found to be ~60%.

4. Results and discussion

4.1 Densification behaviour during HIP process

Figure 6, Figure 7 and Figure 8 show the simulation results of the temperature and pressure distribution in the consolidated demonstrator, as well as the densification during HIPping. Two intermediate stages were chosen for the analysis. One is at time $t=12000$ s, within the temperature and pressure ramping stage, and the second is at $t=14000$ s, within the holding stage of the HIPping cycle. Figure 6(a) illustrates the temperature distribution of part being HIPped at $t=12000$ s which is a result of the heat applied on the exterior of tooling in form of temperature load. The figure 6 shows that the temperature distribution is not uniform. At this stage, the applied temperature is about 1050 °C. The effect of this load can be seen in the temperature gradients in the powder compact. The applied heat is transferred from the surface of the tooling into the powder by conduction. Hence, the outer surface becomes hotter and densifies faster than the inner part, which promotes heat conduction through the sintered layer. The temperature difference between the outer surface and the centre of the powder was found to be ~ 125 °C. The reason for this difference can be attributed to the difference between both the thermal conductivity and heat capacity of the powder and those of the mild steel tooling. In particular, at this stage of the HIP cycle, the thermal conductivity of IN718 powder is $15.1 \text{ Wm}^{-1}\text{K}^{-1}$, compared to $36.6 \text{ Wm}^{-1}\text{K}^{-1}$ at the consolidated state, while it is $30 \text{ Wm}^{-1}\text{K}^{-1}$ for the mild steel tooling. On the other hand, at $t = 14000$ s, the temperature

distribution is uniform as the consolidation has already occurred and the thermal conductivity of IN718 is closer to that in the solid state, Figure 6(b).

Figure 7(a) shows the resultant pressure distribution at $t = 12000$ s. Although the pressure applied on the exterior of the mild steel container is hydrostatic, the developed pressure in the powder part is not hydrostatic, Figure 7. This behaviour is enhanced by the stiffness of the tooling carry on the pressure load that should be otherwise transmitted into the packed powder. The maximum value of pressure predicted by the simulation at 14000 s is 176MPa and the minimum value is 123MPa , whereas the external pressure load at that time is 140MPa . This increase in the developed pressure can be explained by the presence of thermal stresses caused by the difference in the thermal expansion of IN718 and AISI 1080 of the tooling. The lowest predicted pressure is always located in the powder mass especially at thick sections. Similar findings were reported by Svoboda and Nasstrom [12].

Figure 8(a) shows the relative density distribution at $t = 12000$ s. As a result of the developed pressure distribution shown in Figure 7(a), the relative densities in the powder configurations are also non-uniform and they vary from 0.670 to 0.725. At this stage, the thermal strain effect on the densification can be noticed. Large thermal gradient will cause thermal strain to compacts. Hence, the surface with high temperature is deformed faster than the inner surface and the average relative density of the external parts is higher than the interior especially at regions with low tooling stiffness (high induced pressure) such as the top and the bottom flanges. The low density of the part may be attributed to the low induced pressure which is difficult to cause particle deformation. Plastic deformation of the powder has not fully developed at this stage. At $t = 14000$ s, the densification rate has a significant improvement. Most of the densification of the powder compact occurred in this stage. This dramatic improvement is caused by the increasing of the applied and induced pressure. The relative density varies from 0.995 at the thick sections such as the ring and the boss to 0.999 at the thin sections such as the cylinder walls. During this stage, the relative density has improved due to the moving of the particles and elimination of the pores in the compacted powder. When the applied pressure increases to the maximum value prior to the start of the holding stage, the maximum value of plastic strain rate is also achieved.

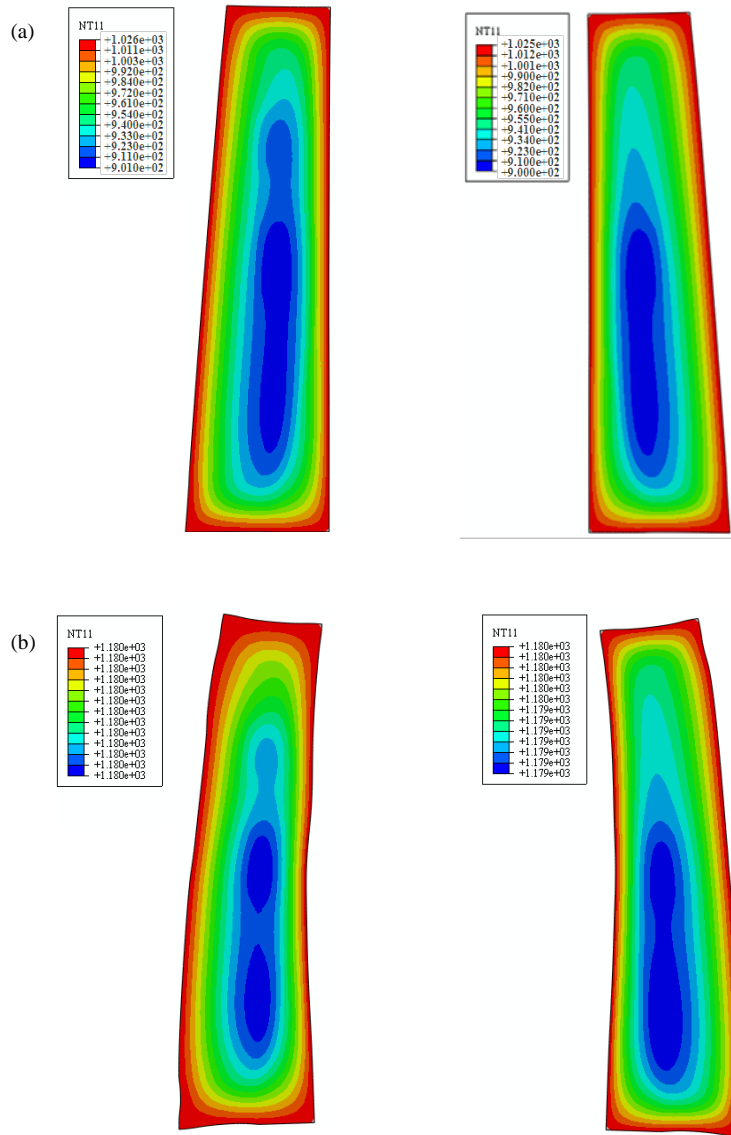


Figure 6. Temperature distribution during HIPping progress in $^{\circ}\text{C}$ (a) at 12000 s, (b) at 14000 s

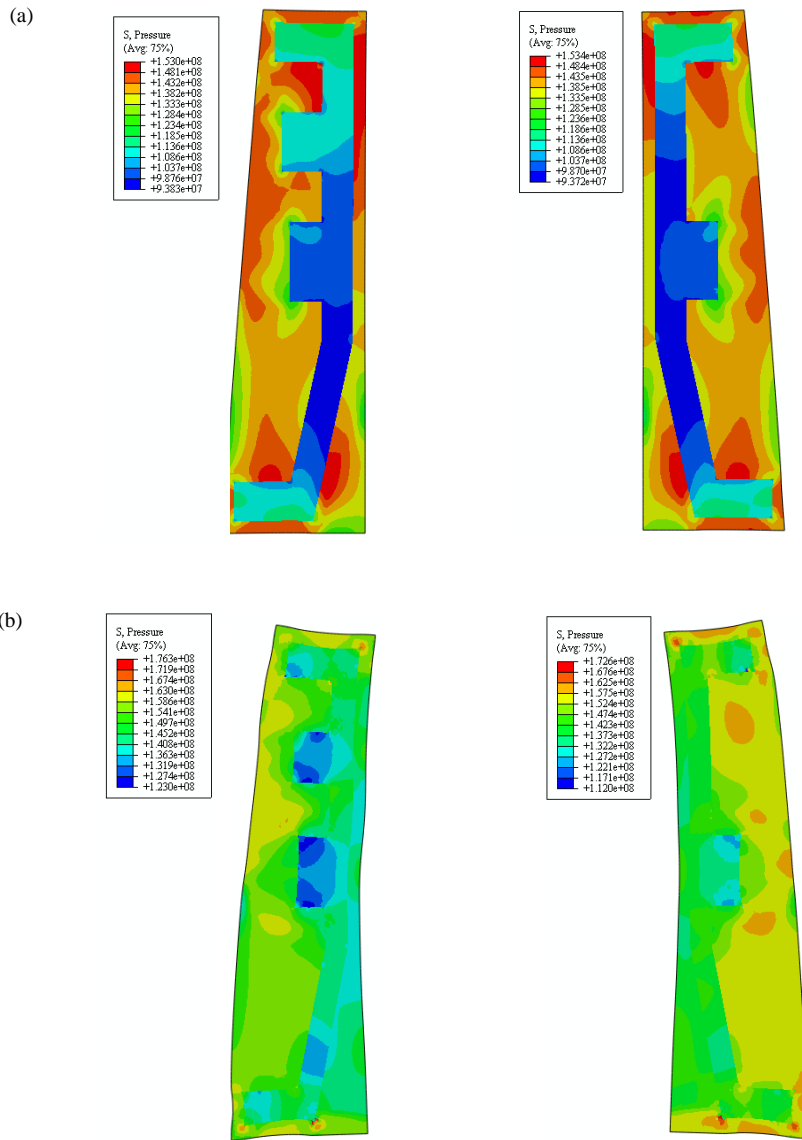


Figure 7. Pressure distribution during HIPping progress in Pa (a) at 12000 s, (b) at 14000 s

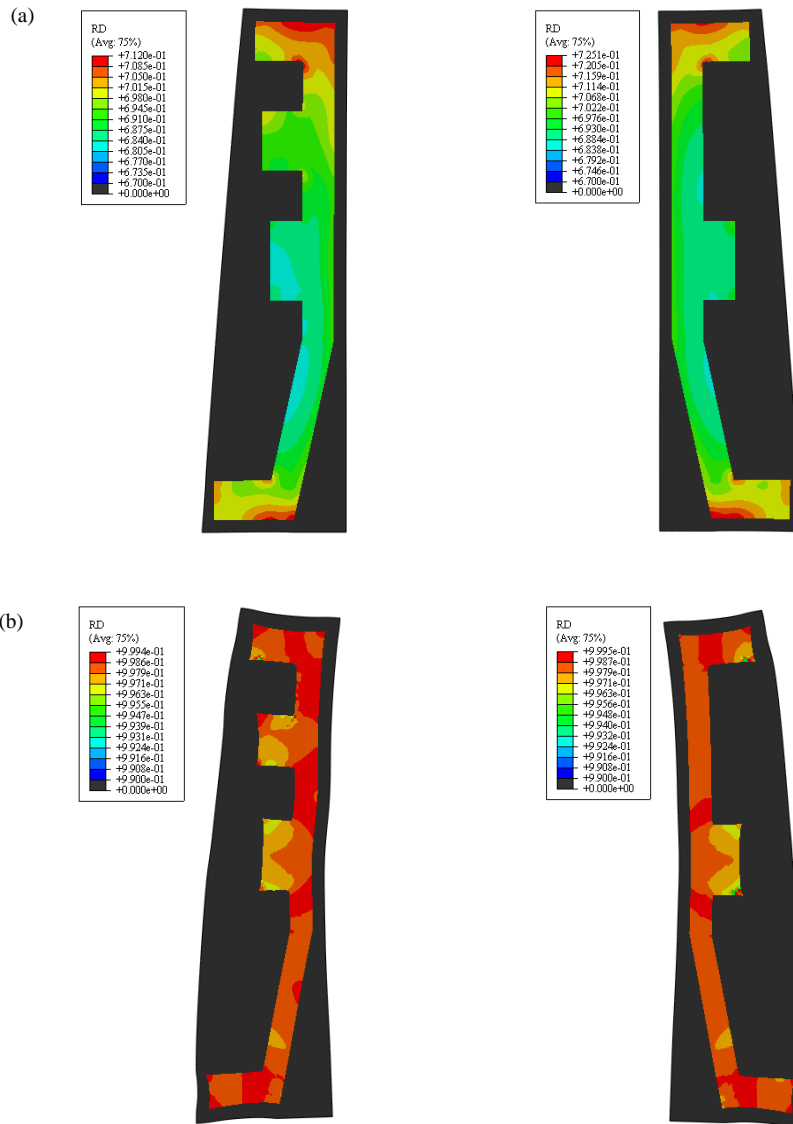


Figure 8. Relative density distribution (a) at 12000 s, (b) at 14000 s

An element in the exterior layer close to the mild steel tooling is chosen to show the evolution of the relative density during the densification and compared to the measured values as shown in Figure 9. The density was measured at three stages; before HIPing (the packing density), at the end of the pressure ramping stage (zero holding time) and after HIPing. The measured values match the predicted ones. However, in the simulation results, the powder becomes fully dense when the maximum temperature and pressure are reached. After that no more powder densification can be recorded. This is due to that the used FE model only accounts for pressure-dependent densification while the time dependent densification is ignored. This is based on the fact that more than 90% of powder densification during HIPping occurs via the instantaneous plastic yield mechanism as reported by Seliverstov *et al.* [16]. As for the measured density, it can be noticed that there is a slight

difference in density between samples measured at zero holding time and samples measured at the end of the HIP cycle this is due the negligible contribution of a typical characteristics of a transient creep stage. During this stage there is a sharp decrease of the equivalent viscoplastic strain rate. The mechanisms of densification at this stage are then attributed mainly to creep, particle re-arrangement, and collapse of the pores. At the end of HIP cycle the relative density is found to be 0.999, which represents almost fully consolidated part. The measured relative density agrees well with that predicted by the FE simulation, at the end of the holding time, with a low underestimated error which makes the simulation results reliable. This will be supported by the results shown in the following section.

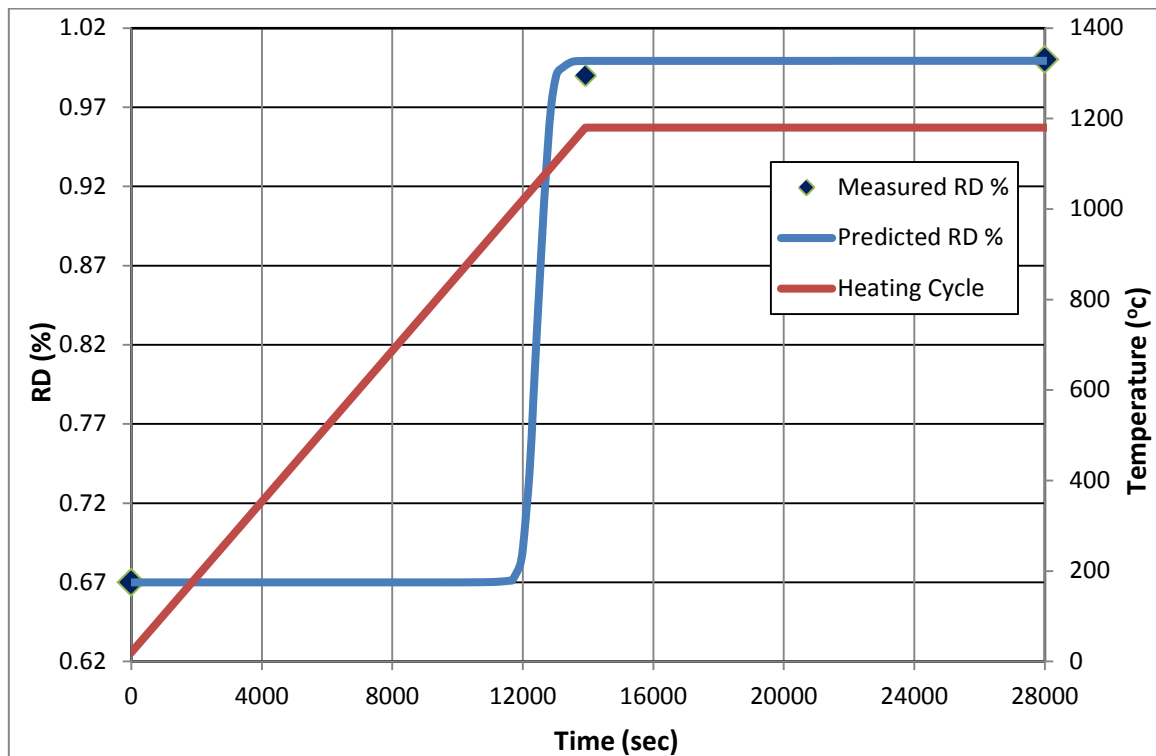


Figure 9. The evolution of relative density (RD) during HIP cycle

4.2 Geometrical analysis and comparison

After 28 iterations, the target geometry of the proposed demonstrator was achieved within $\pm 1\%$. The average computational time of each iteration, using a single core with Intel (R) Core(TM) i7-3820 CPU @ 3.60GHZ and 48 GB RAM, was 11 minutes and the total computational time was 5 hours. An important stage of the proposed approach is the verification of the predicated geometry in comparison with the final one of the manufactured demonstrator shown in Figure 5(c) which is extracted using geometrical scanner. The comparison between the two geometries is illustrated in Figure 10. The radial and axial shrinkage are significantly different for the final product. In particular, the axial shrinkage of the powder is larger than the radial one and the reduction in height is about 7% while the reduction in diameter is about 4%. The axial shrinkage is uniform along the radial direction while the radial shrinkage is less uniform along the axial direction especially at the outer corners of the flanges. Less radial shrinkage can be seen at inner corners of the flanges. This discrepancy may be due to a number of factors, such as the directional stiffness variation of

the mild steel tooling and the non-uniform pressure distribution during HIPping. In general, there is a good agreement between predicted FEA model and measured geometry. The maximum deviation between the FE profile and the experimental one is 0.9 mm which is found at the lower corner. Although the material model that has been used is relatively simple, good prediction of the final geometry is achieved. The simulation time of this model is quite fast as compared with other complicated models [10, 11, 13, 21]. Therefore, the proposed iterative solver can be used as a fast route for container design if optimal HIP cycle is used.

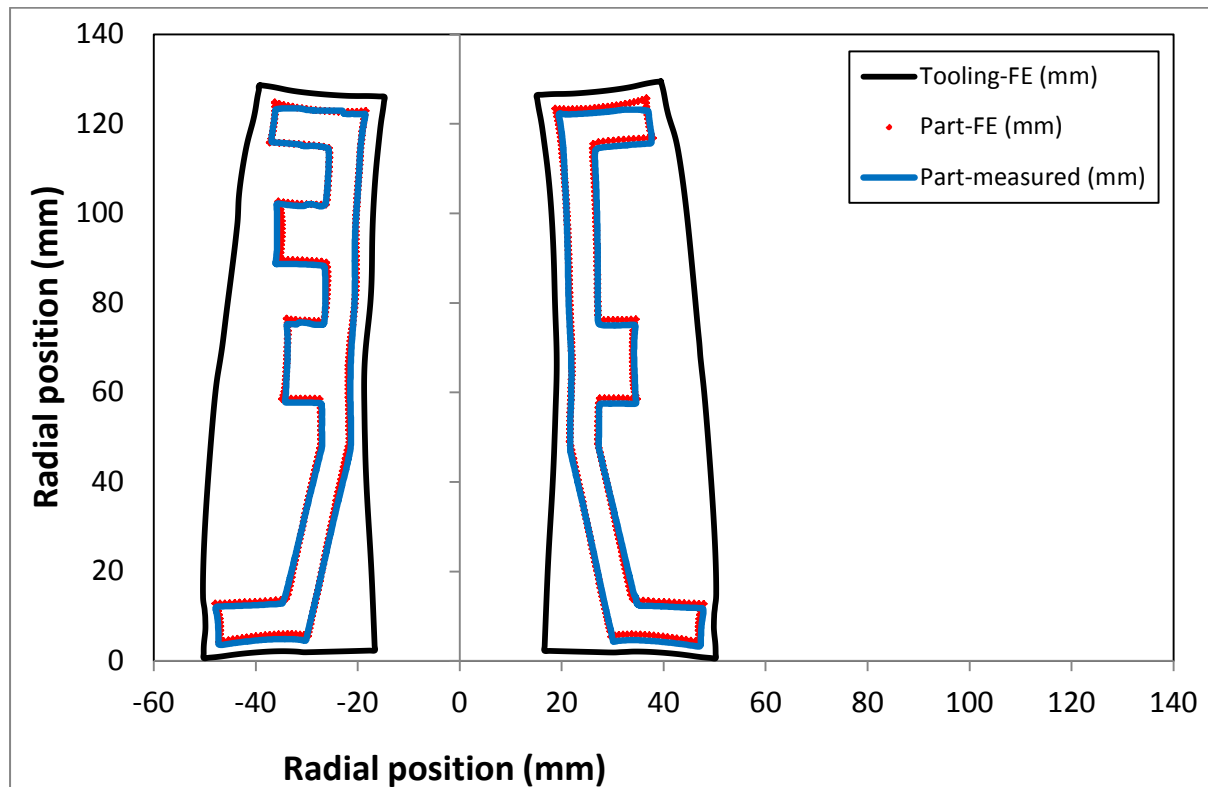


Figure 10. Comparison between geometry obtained from the FE simulation (red dots) and the experimental measurement (blue line) of a cross section passing through the boss, the black line represents the tooling geometry after HIPping

4.3 Microstructural Characterisation

Figure 11 shows the effect of holding time on the porosity-content in as-HIPped IN718 samples. It can be seen that the effect of the holding time on the percentage of the porosity can be neglected. This agrees with the observation reported by Yuan *et al.* [15]. When zero holding time is used, the percentage of porosity is found to be 0.23% which represents 99.77% consolidation, see Figure 11(a). When 4 hours holding time is used, the percentage of porosity is found to be 0.04% which represents 99.96 % consolidation, see Figure 11 (b). This indicates that the time-dependent (creep) mechanism has a minor effect on the densification of the IN718 alloy and that plastic deformation mechanism seems to be dominant in case of the IN718 HIPping which justifies the material model used in this paper. This could be a result of the very large particle size of powder along with the relatively higher temperature and pressure. Therefore, the effect of the holding time on the

microstructure of the HIPped part cannot be neglected and not considered in this investigation.

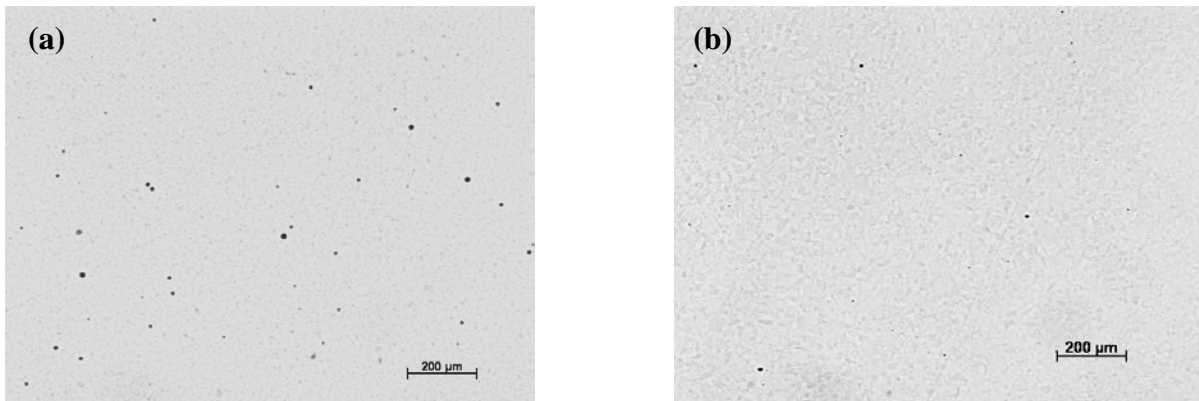


Figure 11. Optical microscopy images showing the porosity after HIPping at (a) zero holding time, (b) 4hrs holding time

5. Summary and Conclusions

In this paper, FE models based on pure plasticity theory of porous metal have been used to simulate HIPping of IN718 superalloy powder. A small demonstrator component has been modelled, designed and produced. Iterative procedure has been used to design the proper tooling for net-shape fabrication of the proposed demonstrator. Experimental analysis has been carried out to validate the FE model, study the effect of the HIPping parameters on the microstructure and to evaluate the time dependent deformation of IN718 superalloy powder during HIPping. The whole process from FEA simulation, feeding the model with experimentally calculated data to geometry verification is performed within the proposed approach.

The principal conclusions from this work are:

- The iterative procedure shown in this paper can be extended directly to improve the design and manufacturing of components with larger and more complex shape made from different materials such as Ti-6Al-4V.
- The plastic collapse model of porous metal can be used for shape prediction. The model is relatively simple and the computational time is quite reasonable.
- Plastic deformation is responsible for more than 99% of the powder consolidation, during HIPping of used IN718 nickel superalloy with the role of creep deformation being minimal.
- The HIPping conditions used in this process are adequate to produce a fully dense nickel based superalloy demonstrator.

Acknowledgements

The work shown in this paper is part of NESMONIC project (Net Shape Manufacture of Ni Superalloy Engine Casing) and was financially sponsored by the Clean Sky Programme.

6. References

- [1] Reed R C (2006) *The superalloys: fundamentals and applications*, Cambridge University Press, Cambridge,
- [2] Shima S, Oyane M (1976) *International Journal of Mechanical Sciences* 18 285-291.
- [3] Cassenti B N (1980) *AIAA J Paper No.* 80-1111.
- [4] Nohara A, Nakagawa T, Soh T, Shinke T (1988) *International Journal for Numerical Methods in Engineering* 25 213-225.
- [5] Abouaf M (1985), *Universite Scientifique et Medical de Grenoble*
- [6] Abouaf M, Chenot J L, G. R, Bauduin P (1986) *Proc. NUMIFORM '86 Conf*, pp. 79-83.
- [7] Abouaf M, Chenot J L, Raison G, Bauduin P (1982) *2nd International Conf. on Isostatic Pressing*.
- [8] Abouaf M, Chenot J L, Raison G, Bauduin P (1988) *International Journal for Numerical Methods in Engineering* 25 191-212.
- [9] Bensson J, Abouaf M (1989) *2nd International Conf. on Isostatic Pressing-Theory and Applications*, Gaitherburg.
- [10] Svoboda A, Håggblad H Å k, Karlsson L (1997) *Computer Methods in Applied Mechanics and Engineering* 148 299-314.
- [11] Svoboda A, Lindgren L-E, Oddy A S (1998) *International Journal for Numerical Methods in Engineering* 43 587-606.
- [12] Svoboda A, Nasstrom M (1996) *Engineering Computations* 13 13-13-37.
- [13] Wikman B, Svoboda A, Håggblad H Å (2000) *Computer Methods in Applied Mechanics and Engineering* 189 901-913.
- [14] Gillia O, Boireau B, Boudot C, Cottin A, Bucci P, Vidotto F, Leibold J M, Lorenzetto P (2007) *Fusion Engineering and Design* 82 2001-2007.
- [15] Yuan W X, Mei J, Samarov V, Seliverstov D, Wu X (2007) *Journal of Materials Processing Technology* 182 39-49.
- [16] Seliverstov D, Samarov V, Alexandrov V, Eckstrom P (1993) *Proceedings of the International Conference on Hot Isostatic Pressing*, Rotterdam.
- [17] Tvergaard V (1981) *International Journal of Fracture* 17 389-407.
- [18] Gurson A L (1977) *Journal of Engineering Material Technology* 2-15.
- [19] Argento C, Bouvard D (1996) *International Journal of Heat and Mass Transfer* 39 1343-1350.
- [20] Wang L, Preuss M, Withers P, Baxter G, Wilson P (2005) *Metallurgical and Materials Transactions B* 36 513-523.
- [21] Jinka A G K, Lewis R W (1994) *Computer Methods in Applied Mechanics and Engineering* 114 249-272.